

# Streptavidin 2D Crystals on Supported Phospholipid Bilayers: Toward Constructing Anchored Phospholipid Bilayers

Ilya Reviakine<sup>†</sup> and Alain Brisson<sup>\*,‡</sup>

Department of Biophysical Chemistry, GBB, University of Groningen, Nijenborgh 4, 9747 AG Groningen, The Netherlands

Received April 30, 2001. In Final Form: September 28, 2001

Streptavidin two-dimensional (2D) crystals were grown on mica-supported phospholipid bilayers containing a biotinylated phospholipid. Their topography structure obtained by atomic force microscopy compares favorably with the electron microscopy analysis of streptavidin 2D crystals grown on lipid monolayers at the air–water interface. The streptavidin 2D crystals were used as a functionalized matrix for anchoring phospholipid bilayers on top of them. Biotinylated liposomes were found to bind specifically to the streptavidin matrix and to transform, locally, into flat lipid surfaces. Height measurements as well as parallel electron microscopy studies performed with biotinylated lipid tubules suggest that the flat lipid surfaces are indeed single lipid bilayers anchored to the ordered streptavidin matrix.

## Introduction

The property of streptavidin, a ~60 kD homotetrameric protein, to present four high-affinity binding sites ( $K_d = 10^{-15}$  M)<sup>1,2</sup> for biotin (vitamin H) is at the origin of widespread biochemical and biotechnological applications.<sup>3,4</sup> The recent use of streptavidin for modifying solid surfaces is related to the growing interest in the fabrication of biocompatible surfaces, an area with direct applications in the fields of biomaterials, biosensors, and nanomaterials. Due to its symmetrical molecular structure,<sup>5,6</sup> streptavidin is able to bind to a biotin-containing surface while exposing two biotin binding sites to the subphase which may be used for immobilizing other biotin-bearing molecules or particles. Most methods reported until now use streptavidin molecules either directly deposited on a surface or specifically bound to biotinylated intermediates, such as self-assembled monolayers<sup>7,8</sup> or protein layers. On the other hand, the well-known ability of streptavidin to self-assemble as 2D crystals at the level of lipid surfaces<sup>9–18</sup> has as yet received little attention in the context of solid-surface modification. Our objective was

therefore to grow 2D crystals of streptavidin on a solid support and to use the ordered streptavidin matrix to anchor biotinylated particles. Most investigations, including those by AFM<sup>19</sup> have concerned the 2D crystallization of streptavidin at the level of lipid monolayers suspended at the air–water interface<sup>9–11,14–18</sup> or the formation of helical arrays of streptavidin at the surface of biotinylated lipid tubules.<sup>20,21</sup> We investigated whether the method we have described recently for the preparation of annexin A5 2D crystals<sup>22</sup> on supported phospholipid bilayers (SPBs)<sup>23–25</sup> could be applied to the streptavidin system.

There are only a few examples of successful attempts to reconstitute functional and mobile transmembrane proteins into SPBs.<sup>26–29</sup> In recent years, attention has

\* Corresponding author. Phone: +33 5 57962216. Fax: +33 5 57962215. E-mail: a.brisson@tecb-polytechnique.u-bordeaux.fr.

<sup>†</sup> Current address: ETH Zurich, Laboratory for Surface Science and Technology (Oberflächentechnik), Wagistr. 2, CH 8952 Schlieren, Switzerland.

<sup>‡</sup> Current address: IECB, University of Bordeaux, 16 rue Pey Berland, F-33607 Pessac Cedex, France.

(1) Chalet, L.; Wolf, F. J. *Arch. Biochem. Biophys.* **1964**, *106*, 1.  
 (2) Green, N. M. *Methods Enzymol.* **1990**, *184*, 51.  
 (3) Wilcheck, M.; Bayer, E. A. *Trends in Biochemical Sciences* **1989**, *14*, 408.  
 (4) Wilchek, M.; Bayer, E. *Anal. Biochem.* **1988**, *171*, 1.  
 (5) Weber, P. C.; Ohlendorf, D. H.; Wendoloski, J. J.; Salemme, F. R. *Science* **1989**, *248*, 85.  
 (6) Hendrickson, W. A.; Pähler, A.; Smith, J. L.; Satow, Y.; Merritt, E. A.; Phizackerley, R. P. *Proc. Natl. Acad. Sci. U.S.A.* **1989**, *86*, 2190.  
 (7) Schmidt, A.; Spinke, J.; Bayerl, T.; Sackmann, E.; Knoll, W. *Biophys. J.* **1992**, *63*, 1385.  
 (8) Spinke, J.; Liley, M.; Guder, H.-J.; Angermaier, L.; Knoll, W. *Langmuir* **1993**, *9*, 1821. Spinke, J.; Liley, M.; Schmitt, F.-J.; Guder, H.-J.; Angermaier, L.; Knoll, W. *J. Chem. Phys.* **1993**, *99* (9), 7012.  
 (9) Blankenburg, R.; Meller, P.; Ringsdorf, H.; Salesse, C. *Biochemistry* **1989**, *28*, 8214.  
 (10) Darst, S. A.; Ahlers, M.; Meller, P. H.; Kubalek, E. W.; Blankenburg, R.; Ribl, H. O.; Ringsdorf, H.; Kornberg, R. D. *Biophys. J.* **1991**, *59*, 387.

(11) Ku, A. C.; Darst, S. A.; Robertson, C. R.; Gast, A. P.; Kornberg, R. D. *J. Phys. Chem.* **1993**, *97*, 3013.  
 (12) Avila-Sakar, A. J.; Chiu, W. *Biophys. J.* **1996**, *70*, 57.  
 (13) Hemming, S. A.; Bochkarev, A.; Darst, S. A.; Kornberg, R. D.; Ala, P.; Yang, D. S. C.; Edwards, A. M. *J. Mol. Biol.* **1995**, *246*, 308.  
 (14) Frey, W.; Schif, W. R.; Vogel, V. T. *Langmuir* **1996**, *12*, 1312.  
 (15) Wang, S.-W.; Poglitsch, C. L.; Yacilla, M. T.; Robertson, C. R.; Gast, A. P. *Langmuir* **1997**, *13*, 5794.  
 (16) Yacilla, M. T.; Robertson, C. R.; Gast, A. P. *Langmuir* **1998**, *14*, 497.  
 (17) Wang, S.-W.; Robertson, C. R.; Gast, A. P. *Langmuir* **1999**, *15*, 1541.  
 (18) Edwards, T. C.; Koppenol, S.; Frey, W.; Schief, W. R.; Vogel, V.; Stenkamp, R. E. Stayton, P. S. *Langmuir* **1998**, *14*, 4683.  
 (19) Scheuring, S.; Müller, D. J.; Ringler, P.; Heymann, J. B.; Engel, A. *J. Microsc.* **1999**, *193*, 28.  
 (20) Ringler, P.; Müller, W.; Ringsdorf, H.; Brisson, A. *Chem. Eur. J.* **1997**, *3*, 620.  
 (21) Huetz, P.; van Neuren, S.; Ringler, P.; Kremer, F.; van Breemen, J. F. L.; Wagenaar, A.; Engberts, J. B. F. N.; Fraaije, J. G. E. M.; Brisson, A. *Chem. Phys. Lipids* **1997**, *89*, 15.  
 (22) Reviakine, I.; Bergsma-Schutter, W.; Brisson, A. *J. Struct. Biol.* **1998**, *121*, 356.  
 (23) Watts, T. H.; Brian, A. A.; Kappler, J. W.; Marrack, P.; McConnell, H. *Proc. Natl. Acad. Sci. U.S.A.* **1984**, *81*, 7564.  
 (24) Watts, T. A.; Gaub, H. E.; McConnell, H. M. *Nature* **1986**, *320*, 179.  
 (25) Sackmann, E. *Science* **1996**, *271*, 43.  
 (26) Salafsky, J.; Groves, J. T.; Boxer, S. G. *Biochemistry* **1996**, *35*, 14773.  
 (27) Cornell, B. A.; Braach-Maksyutis, V. L. B.; King, L. G.; Osman, P. D. J.; Raguse, B.; Wieczorek, L.; Pace, R. J. *Nature* **1997**, *387*, 580.  
 (28) Heyse, S.; Ernst, O. P.; Dienes, Z.; Hofmann, K. P.; Vogel, H. *Biochemistry* **1998**, *37*, 507.  
 (29) Bieri, C.; Ernst, O. P.; Heyse, S.; Hofmann, K. P.; Vogel, H. *Nat. Biotechnol.* **1999**, *17*, 1105.

focused on bilayers decoupled from the solid support by a polymer cushion<sup>30,31</sup> or tethered to it via long, hydrophilic spacers.<sup>27–29</sup> In this study, streptavidin 2D crystals formed on an SPB are investigated as a potential support for anchoring a lipid bilayer.

### Experimental Section

**Materials.** Phospholipids—99% pure egg yolk phosphatidylcholine (EggPC), dioleoyl phosphatidylcholine (DOPC), dioleoyl phosphatidylserine (DOPS), and dipalmitoyl phosphatidylcholine (DPPC)—were purchased from Avanti Polar Lipids (Alabaster, Alabama). DPPE-*lc*-biotin was purchased from Pierce (Illinois). Recombinant streptavidin was from Boehringer Mannheim (Germany).

Other chemicals were purchased from Merck (Germany) or Sigma. Water used throughout this study was purified with a MilliQ water purification system (Millipore). Glassware used in this study was stored overnight in a mixture of chromic and sulfuric acids and rinsed thoroughly with water prior to use.

Buffers contained (A) 2 mM CaCl<sub>2</sub>, 150 mM NaCl, 10 mM HEPES, 3 mM NaN<sub>3</sub>, pH 7.4, and (B) 80 mM KCl, 10 mM Tris-HCl, pH 8.0.<sup>19</sup> They were filtered through a 200 nm syringe filter (Schleicher and Schuell, Germany) prior to use.

**Methods. Preparation of Unilamellar Lipid Vesicles.** Multilamellar vesicles (MLVs) were obtained by mixing appropriate amounts of lipids dissolved in chloroform or chloroform/methanol (2:1, v/v) and evaporating the solvent with argon. After a further 30–40 min of drying in a desiccator connected to a rotary vacuum pump, the lipids were resuspended at the required concentration in the desired buffer by vortexing. Unilamellar vesicles were produced from the MLV suspension by extrusion (EUVs) with a Lipofast extruder (Avestin, Inc., Ottawa, Canada) through 50 nm diameter filters. Both vortexing and extrusion were done at a temperature above the transition temperature of the lipids used to make the vesicles.

**Preparation of SPBs and 2D Crystallization of Streptavidin.** Mica plates (12 mm in diameter, Metafix, Montdidier, France) were used as solid supports for the formation of SPBs and AFM observations. They were glued to metal disks coated with Teflon adhesive tape (“BYTAC”, Norton Performance Plastics Corporation, Ohio) using Rapid epoxy glue according to the procedure described in ref 32. The mica was then cleaved with scotch tape and used immediately. To prepare SPBs, 100 μL of EUVs composed of a mixture of DOPC, DOPS, and DPPE-*lc*-biotin (7:2:1 weight ratio) at ~0.03 mg/mL in buffer A was incubated on mica in a constant humidity chamber at room temperature for 1–2 h, followed by incubation at 60 °C for 30–60 min, after which the sample was washed with buffer A (at room temperature).

2D crystallization of streptavidin on biotin-containing SPBs was performed by injecting streptavidin dissolved in buffer A into the subphase at a final concentration of ~0.1 mg/mL and incubating for 10–60 min.

**AFM.** AFM observations were performed using a Nanoscope IIIa-MultiMode atomic force microscope (Digital Instruments, Santa Barbara, CA) equipped with an “E” (16 μm) or a “J” (120 μm) scanner. The contact mode fluid cell (Digital Instruments) was washed extensively with water, with 95% ethanol, and again with water before each experiment. O-rings, washed overnight in 1% Helmanex solution (GMBH, Germany) and sonicated three times in ultrapure water, were used in experiments in which temperature variation was required.

To perform heating experiments, the microscope was placed in an oven. The temperature inside the fluid cell was verified by observing the melting of DPPC domains in DPPC/DOPC mixed SPBs (cf. refs 33 and 34), which occurred in the range 42–44 °C.

The microscope was allowed to thermally equilibrate for a minimum of 30 min before imaging.

Images were recorded in constant force mode using oxide sharpened silicon nitride tips mounted on cantilevers with a nominal force constant of 0.06 N/m, at scanning rates of 8–15 Hz. The scan angle was 90°. The force was kept at the lowest possible value by continuously adjusting the set point during imaging.<sup>32</sup> Both trace and retrace signals were acquired and compared. Images were flattened and plane-fitted as required.

The topographic maps of streptavidin 2D crystals were calculated from AFM images transferred to a Silicon Graphics workstation using standard Fourier methods.

**Electron Microscopy (EM).** 2D crystals of streptavidin were grown on biotin-containing lipid monolayers at the air–water interface, as previously described.<sup>10,35</sup> 2D projection maps were calculated according to standard Fourier methods.

The data concerning the binding of biotinylated liposomes to helical arrays of streptavidin formed on biotinylated lipid tubules are taken from a previous study.<sup>20</sup>

For EM, specimens were negatively stained with either 1% uranyl acetate, pH 3.5, or 2% sodium phosphotungstate solution, pH 7.5.

### Results and Discussion

**Preparation of Streptavidin 2D Crystals on SPBs Containing Biotinylated Phospholipids.** Continuous SPBs could not be prepared on mica from extruded (or sonicated) liposomes containing mixtures of DOPC and DPPE-*lc*-biotin. Typically, single bilayer disks with associated liposomes were observed, indicating that DPPE-*lc*-biotin does not interfere with liposome adsorption or rupture. Hence, to form SPBs containing DPPE-*lc*-biotin, this lipid was introduced into the DOPC/DOPS (4:1 w/w) mixture which has previously been shown to form continuous SPBs and to support growth of annexin A5 2D crystals.<sup>22</sup> Addition of as little as 10% of the biotin-bearing lipid necessitated a significant change in the SPB preparation procedure as compared to the protocol used to form DOPC/DOPS SPBs (see Experimental Section). The resulting bilayers still contained a significant number of defects (Figure 1A), as opposed to SPBs prepared from the mixture containing no DPPE-*lc*-biotin<sup>22</sup> and from other phospholipids, which are nearly defect-free.<sup>33,36</sup>

The inability to form continuous SPBs from the DOPC/DPPE-*lc*-biotin mixture and the presence of defects in the SPBs prepared from the ternary mixture with DOPS indicates that DPPE-*lc*-biotin inhibits to some extent the coalescence between single bilayer disks.<sup>36</sup> It is likely that, because of their large headgroup area, DPPE-*lc*-biotin molecules accumulate at the edges of single bilayer disks, effectively stabilizing them against fusion with adsorbing liposomes and coalescence with neighboring disks. Our results suggest that the addition of DOPS counteracts this effect to an extent sufficient to allow the formation of a continuous SPB, but defects remain—presumably resulting from the accumulation of DPPE-*lc*-biotin molecules at the edges. A more detailed investigation is required to substantiate this hypothesis further.

2D crystals of streptavidin were observed on biotin-containing SPBs after addition of streptavidin (Figure 1). The coverage of the SPB surface with streptavidin crystals varied between 50% and 90%. The presence of SPB areas (white asterisk in Figure 1A) not covered by crystals (black asterisk in Figure 1A) allowed the average height of the latter above the SPB to be measured:  $3.1 \pm 0.8$  nm ( $n = 61$ ). The histogram of height values is shown in Figure

(30) Majewski, J.; Wong, J. Y.; Park, C. K.; Seitz, M.; Israelachvili, J. N.; Smith, G. S. *Biophys. J.* **1998**, *75*, 2363.

(31) Seitz, M.; Ter-Ovanesyan, E.; Hausch, M.; Park, C. K.; Zasadzinski, J. A.; Zentel, R.; Israelachvili, J. N. *Langmuir* **2000**, *16*, 6067.

(32) Müller, D. J.; Amrein, M.; Engel, A. *J. Struct. Biol.* **1997**, *119*, 172.

(33) Mou, J.; Yang, J.; Shao, Z. *J. Mol. Biol.* **1995**, *248*, 507.

(34) Shao, Z.; Yang, J.; Somlyo, A. P. *Annu. Rev. Cell. Dev. Biol.* **1995**, *11*, 241.

(35) Brisson, A.; Bergsma-Schutter, W.; Oling, F.; Lambert, O.; Reviakine, I. *J. Cryst. Growth* **1999**, *196*, 456.

(36) Reviakine, I.; Brisson, A. *Langmuir* **2000**, *16*, 1806.

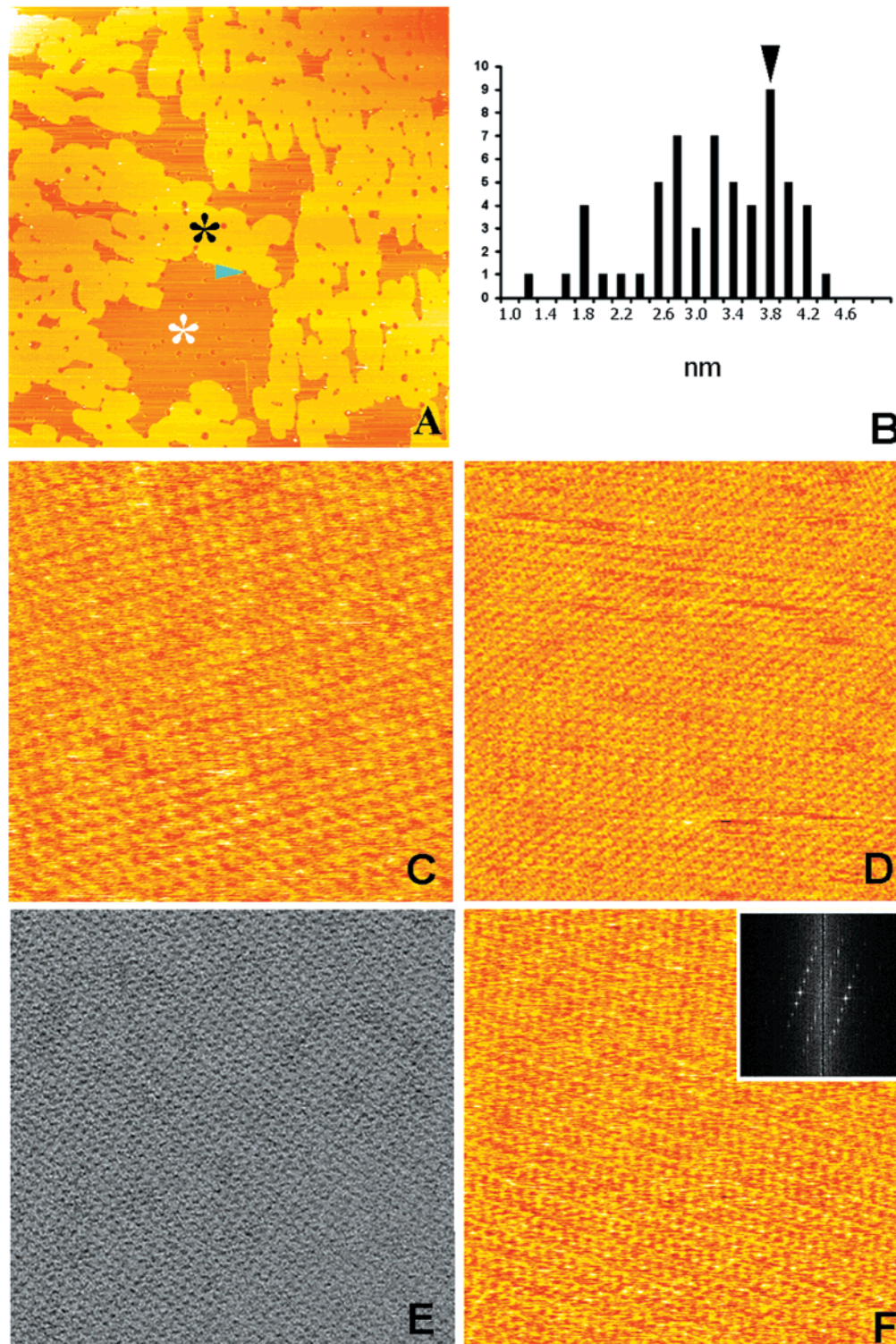


**Figure 1.** (A) 2D crystals of streptavidin grown on an SPB containing 10% DPPE-*l*c-biotin. The biotinylated SPB surface (white asterisk) is covered—partially—with streptavidin crystalline domains (black asterisk). This image was obtained after incubating a 0.1 mg/mL streptavidin solution on an SPB composed of DOPC, DOPS, and DPPE-*l*c-biotin (7:2:1 molar ratio) for ~30 min. The SPB contains a number of defects (holes). The defects are seen to persist in the crystals. Scan size (*z*-scale): 40  $\mu$ m (25 nm). Imaged in buffer A. (B) Histogram of height of streptavidin 2D crystals over the SPB surface. The number of measurements in each class (classes are shown under the abscissa; 0–1 nm, 1–1.2 nm, etc.) is shown along the ordinate. The black arrowhead points to the mode of the distribution. The presence of disordered, mobile, streptavidin molecules surrounding the crystalline areas is thought to be responsible for the spread of the curve at low height values. (C) AFM image of a streptavidin crystalline domain grown on an SPB prepared in an identical fashion to that shown in part A. After crystallization was completed, buffer A was exchanged with buffer B,<sup>19</sup> in which this image was recorded. In this image, each individual streptavidin molecule is revealed as a globular motif. Scan size (*z*-scale): 150 (3) nm. (D) High magnification AFM image of one of the domains shown in part A. Scan size (*z*-scale): 220 (2) nm. (E) 276  $\times$  276 nm<sup>2</sup> EM image of a negatively stained streptavidin 2D crystal grown on a lipid monolayer at the air–water interface. The overall aspect is similar to that of many AFM images, such as the one shown in part D. (F) AFM image of a streptavidin crystalline domain with its Fourier transform (inset) corresponding to the p2 crystal form. Lattice parameters:  $a = 11 \pm 0.1$  nm,  $b = 5.6 \pm 0.1$  nm,  $\gamma = 105 \pm 2^\circ$  ( $n = 3$ ). Imaged in buffer A. Scan size (*z*-scale): 250 (3) nm.

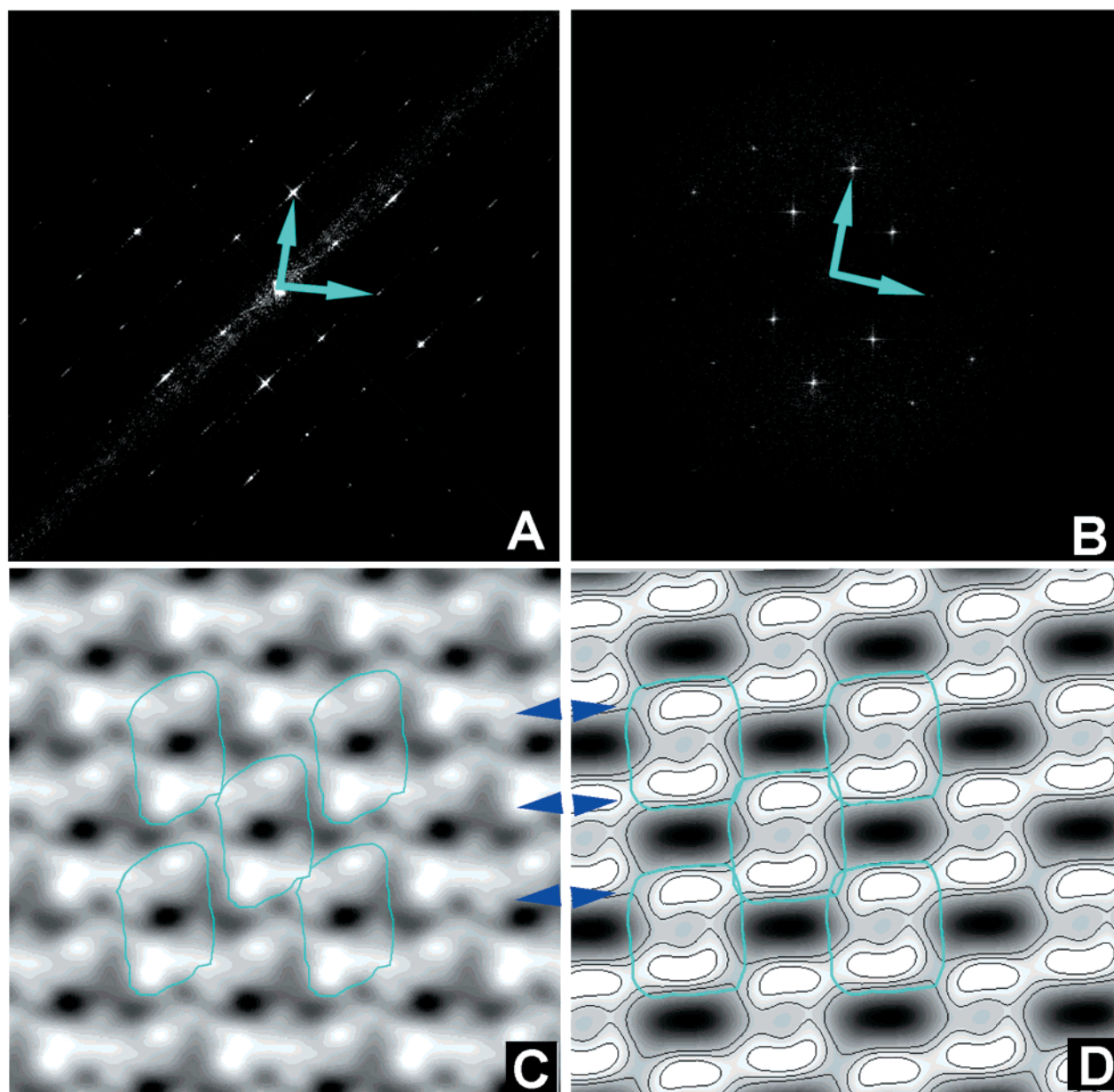


**Figure 2.** (A and B) Fourier transforms of the AFM (A) and EM (B) images shown in Figure 1D and E, respectively. Reciprocal lattice vectors, pointing to the (2, 0) and (0, 2) reflections, are represented with turquoise arrowheads. The lattice constants were as follows: AFM,  $a = b = 8 \pm 0.2$  nm,  $\gamma = 93.2^\circ \pm 0.4^\circ$ ,  $n = 5$  (the lattice vectors are chosen by reference to the EM images (Figure 2B)); EM,<sup>35</sup>  $a = 8.3$  nm,  $b = 8.5$  nm,  $\gamma = 90^\circ$ . The deviation of AFM unit cell parameters from those obtained by EM is most likely due to residual drift. (C) Average topography map of a streptavidin 2D crystal determined from the analysis of part A. Five molecules—four at the corners and one in the middle of a  $c222$  unit cell—are outlined in turquoise. (D) 2D projection map calculated from the EM image shown in Figure 1E. For comparison with part C, five molecules are also outlined in turquoise. Blue arrowheads indicate rows of continuous protein density apparent in both 2D maps.

1B. Contrary to the expected Gaussian distribution, a shoulder is present at the lower height range, while the upper limit is consistent with the expected height of  $\sim 4$  nm.<sup>5,6</sup> One likely reason for the values at the lower end of the distribution is the presence of streptavidin molecules in a disordered phase around the crystals.<sup>18</sup>

The crystalline organization of streptavidin molecules was readily apparent on AFM images (Figure 1C, D, and F). Most of the images (Figure 1C and D), recorded both in the presence and in the absence of  $\text{Ca}^{2+}$ , exhibited crystals with lattice constants  $a = b = 8 \pm 0.2$  nm,  $\gamma = 93.2^\circ \pm 0.4^\circ$ , consistent with those of the  $c222$  crystal form (Figure 2)<sup>37</sup> expected in this pH range.<sup>16</sup> Typical Fourier transforms showed diffraction peaks extending to  $1/1.5$  nm<sup>-1</sup> (Figure 2A). The overall aspect of the AFM images was found to be rather variable, however (compare for

example Figure 1C and D). In addition, a small number of images obtained in the presence of  $\text{Ca}^{2+}$  exhibited Fourier transforms consistent with a  $p2$  crystal form (unit

(37) The crystal forms are named here following the nomenclature used in the literature.<sup>11,12,16</sup> It should be noted that  $c222$  is the symmetry of the 2D crystal itself. In projection, the in-plane 2-fold rotational axes become mirror axes, and the symmetry of the projection map is  $cm\bar{m}$ . The molecule itself possesses  $D_2$  ( $222$  in the international system) point group symmetry (Atkins, P. W. *Physical chemistry*; W. H. Freeman and Company: New York, 1990; pp 428–429). As AFM reveals only the surface topography, AFM images possess  $p2$  symmetry. Departure from  $p2$  symmetry is likely to be due to tip-sample interactions. Such a reduced symmetry is also noticeable in the 2D projection maps derived from EM images of negatively stained 2D crystals grown on lipid monolayers at the air-water interface and should result from a difference in staining between the molecules located close to the lipid film and the molecules facing the aqueous subphase (cf. Figure 2D).

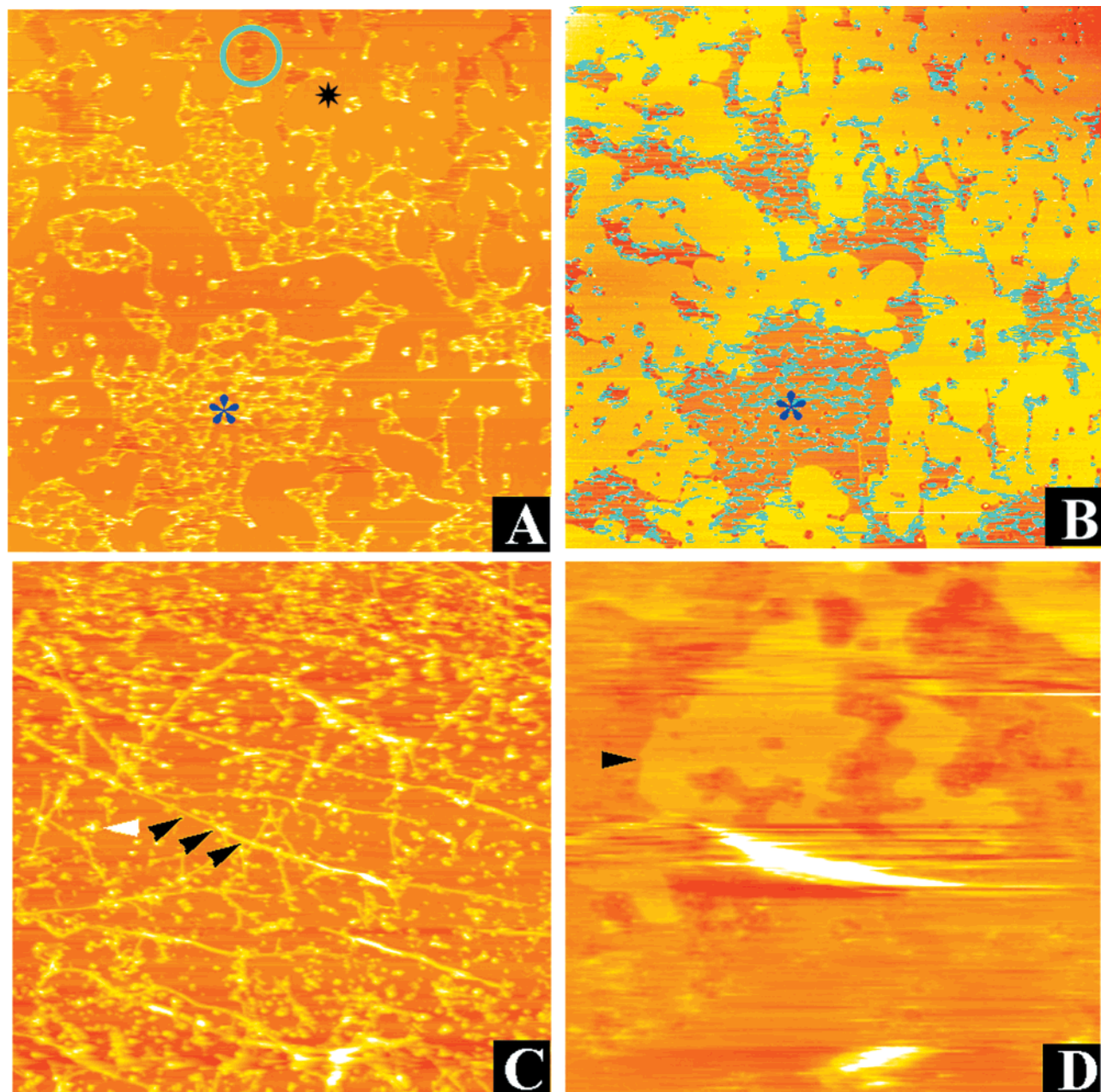


**Figure 3.** (A) Same area as shown in Figure 1A, after the addition of DMPC/DPPE-*lc*-biotin (9:1 wt ratio) vesicles to the preheated specimen, at 34 °C. Flat areas (black asterisk), which correspond to the areas in Figure 1A covered by the crystals (see B), are surrounded by defects (one is encircled in turquoise), most of which contain liposomes forming netlike structures (blue asterisk in parts A and B). The depth of the defects where liposomes were absent is about 9.9 nm. Scan size (*z*-scale): 40  $\mu\text{m}$  (150 nm). Imaged in buffer A. (B) In this image, the liposome-containing areas from part A were selected and overlaid (in turquoise) over Figure 1A. Isolated liposomes are found at the level of the defectuous holes while aggregated liposomes form netlike structures in the large areas from Figure 1A not covered by the crystals. Scan size: 40  $\mu\text{m}$ . (C) DMPC/ $G_{MI}$ /DPPE-*lc*-biotin (8:1:1 wt ratio) 100 nm vesicles, extruded at 40 °C, were added to the streptavidin 2D crystals. The long threadlike objects (black arrowheads) are lipid tubules. The white arrowhead indicates an adsorbed liposome. Similar images were obtained after addition of DOPC/DOPS/DPPE-*lc*-biotin (7:2:1 wt ratio) to the streptavidin crystals (not shown). Scan size (*z*-scale): 25  $\mu\text{m}$  (300 nm). (D) After addition of DPPC/DPPE-*lc*-biotin (6:4 wt ratio) liposomes at 34 °C, heating the specimen to 40 °C, and cooling to room temperature, objects which are interpreted as single bilayer disks (arrowhead) covering the crystalline layer were observed. The height of these disks over the surrounding surface was  $\sim 6$  nm. Scan size (*z*-scale): 4  $\mu\text{m}$  (84 nm).

cell dimensions  $a = 11 \pm 0.1$  nm,  $b = 5.6 \pm 0.1$  nm,  $\gamma = 105^\circ \pm 2^\circ$ ) observed previously by EM<sup>15</sup> (Figure 1F).

It is noteworthy that the AFM images exhibited a strikingly similar aspect to EM images of negatively stained streptavidin 2D crystals (compare Figure 1D and E). The respective Fourier transforms (Figure 2A and B) are also similar, although the intensity distributions of the diffraction peaks are different. Despite the different appearance of the average topography map calculated from

the AFM images (Figure 2C) and the 2D projection map calculated from the EM data (Figure 2D<sup>35</sup>), similar features can be recognized—such as rows of continuous protein density (blue arrowheads) separated by rows of lower and discontinuous protein density. A tentative assignment of the molecular boundary on the topography map is shown in Figure 2C with turquoise contours.

It is also interesting to note that although some of the crystals observed exhibit an anisotropic morphology

(Figure 1A), no X-shaped crystals, such as those typically visible at the air–water interface by fluorescence<sup>9</sup> or Brewster angle<sup>14</sup> microscopy, were observed. Liposomes and/or lipid tubules were frequently found associated with the crystals.

**Preparation of Anchored Phospholipid Bilayers (APBs).** In the preceding section it was established that streptavidin 2D crystals grew on SPBs containing a biotinylated phospholipid. Their ability to serve as a functional matrix for immobilization of biotinylated liposomes and to support formation of anchored phospholipid bilayers (APBs) in a process analogous to the formation of SPBs by vesicle fusion<sup>23,24,36</sup> will now be discussed.

Liposomes containing DPPE-*lc*-biotin in mixtures with DPPC, DMPC, DMPC/ $G_{M1}$ , DOPC, or DOPC/DOPS were found to bind specifically to streptavidin 2D crystals (Figure 3). With liposomes containing DPPC or DMPC—that is, phospholipids which are in solid (liquid condensed) phase at room temperature—flat objects, consistent in appearance with single bilayer disks, either appeared on the crystals spontaneously or were induced by a brief heating/cooling cycle (Figure 3B and D). On the contrary, no such objects were observed when mixtures containing fluid phase lipids were used; the liposomes remained intact. The height of the flat structures—referred to as APBs from now on—was analyzed by measuring either the depth of defects in them or their height relative to the underlying surface at their border. The depth of the holes in continuous APBs (Figure 3A) was found to be  $9.9 \pm 1$  nm ( $n = 50$ ). This value is consistent with the hypothesis that defects in APBs correspond to areas where the underlying SPB is not covered with a streptavidin crystal. The height of the isolated disks (precursors of a continuous APB, such as those shown in Figure 3D) was  $\sim 6$  nm, in the range expected for the height of a single bilayer on top of a crystal. The presence of a meshwork of liposomes associated with the large areas devoid of streptavidin crystals (blue asterisk in Figure 3A and B) is likely to be due to the presence of bound streptavidin molecules randomly distributed on the underlying SPB.

**EM of Complexes Formed between Biotinylated Liposomes and Helical Arrays of Streptavidin Formed on Biotinylated Lipid Tubules.** The formation of APB on top of an ordered planar matrix of streptavidin is reminiscent of a previous study in which we investigated the binding of biotinylated liposomes to helical arrays of streptavidin.<sup>20</sup> Some results of this study deserve to be reconsidered here because this system provides a complementary side-view observation of the multilayered system imaged by AFM from the top. In this study,<sup>20</sup> the spontaneous formation of lipid tubules made of a mixture of biotinylated dioctadecylamine (DODA-EO<sub>2</sub>-biotin) and DOPC (1:4 molar ratio) was described and it was shown that streptavidin molecules assembled into ordered helical arrays at the tube surface. Figure 4A presents a typical image of a lipid tube covered with a helical array of streptavidin.

Liposomes made of DPPE-*lc*-biotin, DOPC, and monosialoganglioside  $G_{M1}$  (1:10:1, molar ratio) were found to associate tightly with the streptavidin layer (Figure 4B). Some liposomes were observed to flatten against the streptavidin layer (arrow). This flattening must result from the establishment of a zipper-like structure between the two “planar” surfaces bearing the biotinylated lipid headgroups and the ordered monolayer of streptavidin molecules placed in between. Some liposomes flattened in such a way that they wrapped totally around the tube (arrowhead).

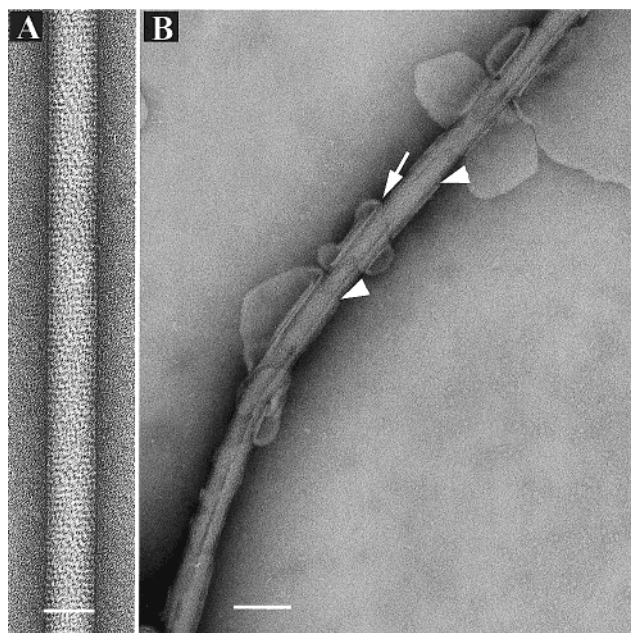


**Figure 4.** Binding of biotinylated liposomes on helical arrays of streptavidin. (A) Electron micrograph of a lipid tubule covered with a helical array of streptavidin molecules. Scale bar: 40 nm. (B) Liposomes containing biotinylated lipids flatten upon binding to a helical array of streptavidin (arrow). Some of them wrap tightly around the tube surface (arrowheads). Scale bar: 100 nm.

These observations enable us to conclude that the flat lipid surfaces observed by AFM covering the streptavidin crystals correspond also to APBs. However, a significant difference is observed between the two systems: the APB imaged by AFM seems continuous, implying that fusion or coalescence has occurred between adjacent ruptured liposomes, while liposomes bound to tubes do not appear to fuse with each other. This different behavior is likely to result from the difference in curvature between the two systems.

## Conclusions

2D crystals of streptavidin were prepared on mica-supported phospholipid bilayers containing a biotinylated phospholipid and could be imaged at submolecular resolution by AFM. The exposed biotin sites on streptavidin were used to anchor biotinylated liposomes. Liposomes containing phospholipids in the liquid-condensed phase gave rise to objects consistent with single lipid bilayers forming on top of the streptavidin crystals. The strategy presented here for the construction of surface-anchored 3D assemblies via specific anchoring to a protein 2D crystalline matrix could serve for numerous applications. Conditions must yet be improved to transform the local APBs into “ideal”, continuous APBs. Various approaches toward achieving this goal could be envisioned. Lipid mixtures of various compositions and phase behavior could be exposed to temperature cycles through the temperature of the solid condensed–solid expanded phase transition. Incorporation of fusogenic lipopeptides<sup>38</sup> within the LUVs to promote the fusion of LUVs after their anchoring is another avenue worth exploring. An alternative strategy would be to use specifically anchored short-chain amphiphiles in order to induce the spontaneous spreading of LUVs, by analogy with the use of mercaptoalkanes on gold surfaces.<sup>28,39</sup>

(38) Pecheur, E. I.; Hoekstra, D.; Sainte-Marie, J. *Biochemistry* **1997**, *36*, 3773.

**Acknowledgment.** We thank Wilma Bergsma-Schutter for her expert assistance with the electron microscopy

and Dr. Philippe Ringler for his original analysis of the biotinylated lipid tubes.

---

(39) Hennesthal, C.; Steinem, C. *J. Am. Chem. Soc.* **2000**, *122*, 8085.

LA010626I